INTERNATIONAL JOURNAL OF ENERGY STUDIES

e-ISSN: 2717-7513 (ONLINE); homepage: https://dergipark.org.tr/en/pub/ijes

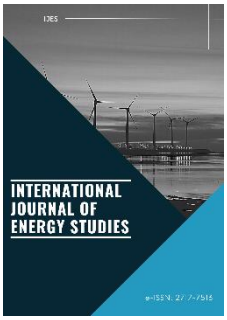

Research Article
Int J Energy Studies 2026; 11(1): 353-370
DOI: 10.58559/ijes.1837526

Received : 07 Dec 2025
Revised : 24 Jan 2026
Accepted : 24 Jan 2026

Electrical and thermal characterization of lead-free Sn-Zn-Cu solder alloys

Esra Öztürk[a,*], Pınar Ata Esener[b], Sezen Aksöz[c]

[a]Kocaeli University, Faculty of Art and Sciences, Department of Physics, 41001, Kocaeli, Türkiye, ORCID: 0000-0002-3531-7564

[b]Nevşehir Hacı Bektaş Veli University, Faculty of Art and Sciences, Department of Physics, 50300, Nevşehir, Türkiye, ORCID: 0000-0002-6498-4534

[c]Nevşehir Hacı Bektaş Veli University, Faculty of Art and Sciences, Department of Physics, 50300, Nevşehir, Türkiye, ORCID: 0000-0002-8990-1926

([*]Corresponding Author:esra.ozturk@kocaeli.edu.tr)

Highlights

- Thermal and electrical behaviors of four Sn-Zn-Cu phases were characterized.
- Thermal conductivity, melting parameters, and electrical conductivity were quantified.
- Results confirm the suitability of Sn-Zn-Cu alloys for Pb-free soldering applications

You can cite this article as: Öztürk E, Ata Esener P, Aksöz S. Electrical and thermal characterization of lead-free Sn-Zn–Cu solder alloys. Int J Energy Studies 2026; 11(1): 353-370.

ABSTRACT

Sn-Zn-Cu alloys have emerged as promising candidates to replace conventional lead-containing solder systems due to their environmentally favorable characteristics. In this study, four different phases within the Sn-Zn-Cu alloy system were investigated in terms of their thermal and electrical properties. Temperature-dependent thermal conductivity was measured using the linear heat-flow method, and the corresponding conductivity coefficients were derived from the collected data. Differential Scanning Calorimetry (DSC) was employed to determine melting temperatures, enthalpies of fusion, and specific heat differences between the liquid and solid phases. Electrical conductivity values were obtained using the four-point probe technique. Compared to commonly used Pb-free solder systems reported in the literature, the investigated Sn–Zn–Cu alloys exhibit a favorable combination of lower melting temperatures, stable thermal behavior, and controlled electrical conductivity, which are critical for ensuring reliable heat dissipation and electrical performance in advanced electronic and energy-related soldering applications. These characteristics highlight the potential of Sn–Zn–Cu alloys as cost-effective and high-performance alternatives to conventional Pb-free solders.

Keywords: Heat transfer, Zinc compounds, Thermal properties, Electrical conductivity

1. INTRODUCTION

Lead-based solder alloys have been widely used for nearly two millennia; however, growing scientific evidence has demonstrated that lead and its compounds pose significant risks to both human health and the environment. The Environmental Protection Agency (EPA) classifies lead and its derivatives among the 17 most hazardous toxic substances due to their severe biological and ecological impacts [1, 2]. Once introduced into the human body, lead interferes with essential protein functions and accumulates over time, resulting in irreversible health complications. Exposure to lead dust or vapors generated during soldering processes has been associated with neurological disorders, reproductive dysfunction, hypertension, reduced hemoglobin synthesis, vasoconstriction, and anemia. Beyond its direct health effects, improper disposal of lead-containing materials contributes substantially to environmental contamination. Consequently, the global shift toward eliminating lead usage has become imperative, and soldering applications, one of the major industrial sources of lead exposure, have received particular focus in the development of alternative, environmentally friendly Pb-free materials [3-7].

As the detrimental effects of lead have become increasingly well understood, lead-free solder systems have gained considerable importance across numerous industrial sectors. Pb-free solder materials are now widely employed in electronic components, metal joining processes, and various metallographic applications [8–17]. Although lead was gradually banned from most electronic products, Pb-based solders continued to be used in automotive electronics for a period due to stringent performance and reliability requirements [9–14]. With the introduction of stricter environmental regulations and a growing emphasis on sustainability, a complete ban on lead in the automotive industry was implemented in 2014, further accelerating the global transition toward Pb-free soldering technologies.

In recent years, this transition has become particularly critical for the energy sector, where electronic reliability, thermal management, and long-term operational stability are of paramount importance. Modern energy systems, including photovoltaic modules, power converters, inverters, battery management systems, and grid-level power electronics, operate under elevated temperatures and cyclic thermal loading conditions. In such applications, solder materials play a crucial role not only in ensuring mechanical integrity but also in governing heat dissipation and electrical signal transmission. Therefore, the development of Pb-free solder alloys with optimized

thermal and electrical properties is essential for improving the efficiency, durability, and safety of energy-related electronic systems [18-21].

Despite substantial progress in the development and adoption of Pb-free solder alloys, challenges related to reliability and long-term performance still persist. Common Pb-free systems such as Sn-Ag-Cu, Sn-Au, Sn-Ag, Sn-Sb, Sn-Zn, and Sn-Cu exhibit several inherent limitations. For example, while Sn-Ag-Cu solders offer good wettability and suitable operational temperatures, the formation of Ag_3Sn intermetallic compounds can reduce mechanical strength and impair creep resistance. In addition, silver is approximately forty times more expensive than tin, significantly diminishing the economic feasibility of the Sn-Ag-Cu system. The Sn-Au system, although used in high temperature applications, suffers from high eutectic temperatures and relatively large wetting angles, restricting its practical applicability.

In Pb-free solder systems, tin serves as the primary element due to its ability to form strong metallurgical bonds during soldering. Among alternative systems, Sn-Zn alloys are widely used in both commercial and industrial applications owing to their excellent mechanical properties [22, 23]. Sn-Cu alloys are commonly employed in electronic packaging, though they remain susceptible to oxidation and corrosion under service conditions [22, 23]. In addition, Sn-Cu alloys also function effectively as soft solders for aluminum and as electroplated coatings for protecting steel surfaces. From an energy-systems perspective, maintaining a melting temperature comparable to that of conventional Pb-Sn alloys is particularly advantageous, as it ensures compatibility with existing manufacturing infrastructure for photovoltaic modules and power electronic assemblies, thereby avoiding costly process modifications [22, 23].

Modern industrial components, devices, and tools, especially those used in energy conversion and transmission systems, are manufactured from a wide variety of materials, including ceramics, glass, metals, and polymers, each with distinct structural and functional requirements. For design engineers working in the energy sector, material selection must balance cost, reliability, thermal management capability, and electrical performance. Achieving an optimal material choice therefore necessitates a comprehensive understanding of the thermal and electrical properties of candidate solder alloys under realistic operating conditions [18-21].

The main goal of this study is to identify a lead-free solder system with improved thermal and electrical properties, while also providing better safety for human health and the environment. In addition, this study aims to provide new thermophysical data for which only limited information is available in the literature. For these purposes, Zn and Cu were added to Sn-based systems [24]. In the present study, thermal and electrical properties of Sn-based Sn-0.28 wt.% Zn-3.60 wt.% Cu, Sn-2.56 wt.% Zn-1.38 wt.% Cu, Sn-6.77 wt.% Zn-7.18 wt.% Cu, and Sn-37.78 wt.% Zn-7.34 wt.% Cu alloys were systematically investigated to determine the optimal Pb-free solder candidate.

2. MATERIALS AND METHODS

2.1. Preparation Of Alloy Systems And Metallographic Processes

Sn–Zn–Cu alloy systems (Sn–0.28 wt.% Zn–3.6 wt.% Cu, Sn–2.56 wt.% Zn–1.38 wt.% Cu, Sn–6.77 wt.% Zn–7.18 wt.% Cu, and Sn–37.78 wt.% Zn–7.34 wt.% Cu) were prepared using high-purity Sn (99.99 wt.%, CAS No. 7440-31-5, Sigma-Aldrich), Zn (99.99 wt.%, CAS No. 7440-66-6, Sigma-Aldrich), and Cu (99.99 wt.%, CAS No. 7440-50-8, Sigma-Aldrich) elements. Graphite crucibles with dimensions of 50 × 12 mm were used for the preparation of samples intended for thermal conductivity, electrical conductivity, and DSC analyses. A schematic illustration of the specimen is shown in Fig. 1 [25]. Approximately 25 cm³ of metal was melted in a graphite crucible inside a vacuum melting furnace, which ensured oxidation-free melting under reduced pressure. The furnace assembly consists of two nested alumina tubes, a vacuum pump, a temperature controller, a variac, and a cooling system [26, 27].

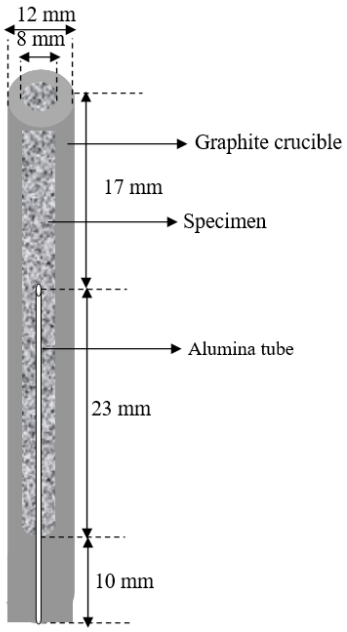

Figure 1. Schematic illustration of specimen

The molten alloys were then poured into graphite crucibles preheated to approximately 50 K above their melting temperatures using a custom-built casting furnace, in order to ensure sufficient fluidity and to minimize premature solidification during casting. This furnace was specifically designed to promote unidirectional solidification by casting the molten alloy into vertically oriented crucibles. Solidification proceeded from the bottom upward, ensuring complete filling of the crucible and minimizing shrinkage defects [26, 27].

After solidification, the alloy rods were removed from the crucibles and sectioned into 30 mm lengths. These specimens were then placed in a linear heat-flow apparatus for thermal conductivity measurement. The ends of each sample (10 mm on both sides) were positioned in hot and cold holders, while a 10 mm central region was left between them to establish a linear temperature gradient and minimize radial heat loss. Temperatures along the sample were monitored using three K-type thermocouples (Ni-Cr/Ni-Al, 0.25 mm diameter) embedded at 2-3 mm intervals. Prior to installation, the thermocouple locations were examined under an optical microscope to accurately determine the distances (ΔX) between them. All thermocouples were placed inside alumina tubes (1.2 mm OD × 1.0 mm ID × 20 mm) and connected to a data-logging measurement system.

Finally, the solidified bars were transversely sectioned into smaller cylindrical specimens (5 mm in length and 8 mm in diameter) using a Micracut 151 precision cutting machine.

2.2. Measurements Of Electrical Conductivity Variations With Temperature

Electrical conductivity is a fundamental property of metallic alloy systems and is influenced by various parameters such as impurities, heat treatment, grain size, and plastic deformation. However, temperature and chemical composition have the most significant effects on electrical conductivity [28]. As temperature increases, lattice vibrations (phonons) become more intense. This enhancement in phonon activity increases the probability of electron scattering, particularly at lattice imperfections, grain boundaries, and substitutional atom sites [29, 30]. The resulting increase in electron-phonon interactions leads to a higher frequency of inelastic scattering events, thereby reducing the electron mean free path. Consequently, the electrical resistance of the metal increases with temperature, while its electrical conductivity decreases.

The temperature dependence of electrical resistivity can be expressed as:

$$\rho(T) = \rho_0[1 + \alpha_{ETC}(T - T_0)] \quad (1)$$

Here, $\alpha_{ETC}$is the electrical temperature coefficient, $T_0$is the reference temperature, and $\rho_0$is the resistivity at the reference temperature T_0. Electrical conductivity is the inverse of electrical resistivity, and its temperature dependence can be expressed as:

$$\sigma = \frac{1}{\rho} = \frac{1}{\rho_0[1 + \alpha_{ETC}(T - T_0)]} = \frac{\sigma_0}{1 + \alpha_{ETC}(T - T_0)} \quad (2)$$

The temperature coefficient of electrical conductivity (α_{ETC}) can be defined as:

$$\alpha_{ETC} = \frac{\sigma_0 - \sigma}{\sigma(T - T_0)} = \frac{1}{\sigma}\ \frac{\Delta\sigma}{\Delta T} \quad (3)$$

In the present study, the temperature dependence of electrical conductivity was measured using the four-point probe method, a widely used technique for determining the electrical conductivity of materials [31]. The schematic diagram of four-point probe system is shown in Fig. 2. The system consists of four equally spaced platinum tips of finite radius, each supported by springs to minimize sample damage during probing. These tips are mounted on an automated mechanical stage that moves vertically during measurements.

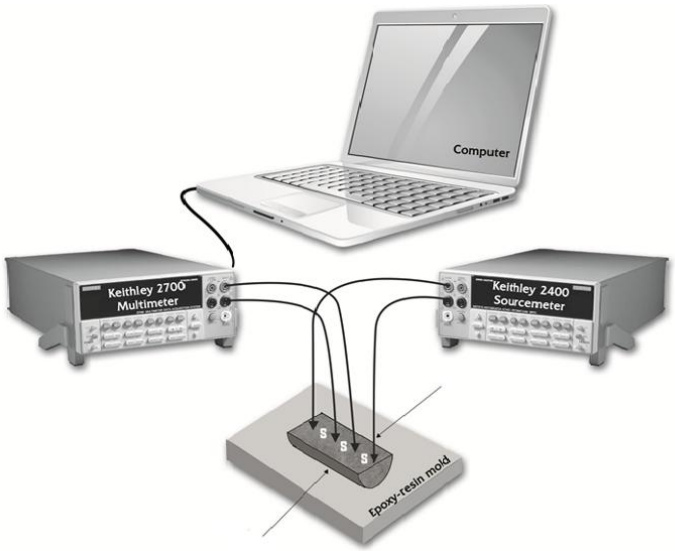

Figure 2. The schematic diagram of four-point probe method used for measuring electrical resistivity/conductivity.

A high-impedance current source supplied current through the two outer probes, while voltage was measured across the two inner probes to determine sample resistance. The four-point probe setup

included a programmable power supply, a multimeter, a Proterm ash furnace, and a computer for data acquisition.

During measurements, the samples were heated from room temperature to approximately 10 K below their respective melting points. A K-type thermocouple (0.5 mm diameter) was used to monitor sample temperature. At each annealing temperature, constant-current and constant-voltage readings were taken repeatedly to ensure measurement accuracy.
The resistivity of the material is expressed as:

$$\rho = \frac{1}{\sigma} = \mathrm{RCF} \cdot \frac{V_{\mathrm{measured}}}{I_{\mathrm{measured}}} \quad (4)$$

Here, RCF is the resistivity correction factor that depends on sample geometry, material thickness, electrode size, and electrode positioning [32]. Current (I) and voltage (V) were measured using the outer and inner probes, respectively. After the temperature dependence of electrical resistivity was obtained, the resistivity values at room temperature were inverted to determine the corresponding electrical conductivity.

In the present work, the temperature-dependent electrical conductivities of Sn–0.28 wt.% Zn–3.6 wt.% Cu, Sn–2.56 wt.% Zn–1.38 wt.% Cu, Sn–6.77 wt.% Zn–7.18 wt.% Cu, and Sn–37.78 wt.% Zn–7.34 wt.% Cu alloys, along with pure Sn, Zn, and Cu were investigated and plotted.

2.3. Measurements Of Thermal Conductivity Variations With Temperature

In this study, the temperature-dependent thermal conductivity of solid samples was determined using a linear heat-flow apparatus. During measurements, one side of the specimen was heated in 20 K increments up to approximately 10 K below its melting point, while the opposite side was cooled to establish a linear temperature gradient. The apparatus consists of three main components: a hot stage, a cold stage, and a sample holder (Fig. 3) [26, 27, 33-38].

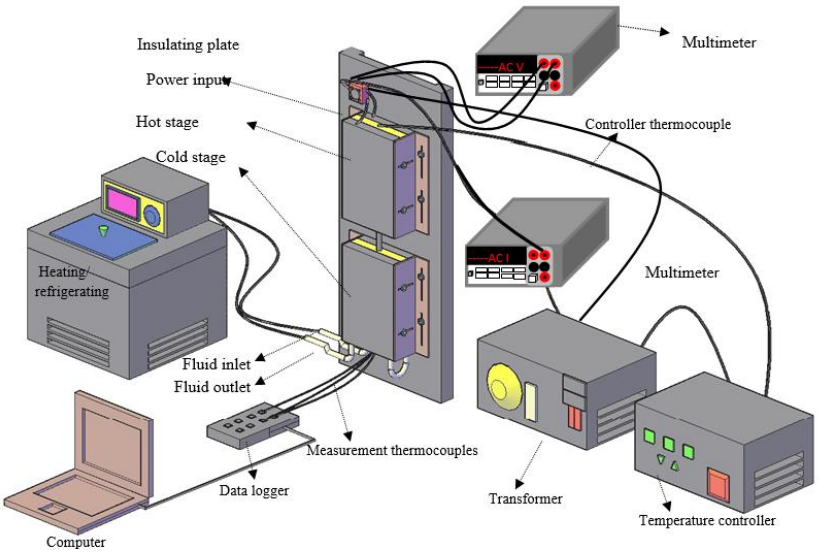

Figure 3. Block diagram of linear heat flow apparatus used for measuring thermal conductivity.

Thermal conductivity (K) was calculated using Fourier's law for one-dimensional steady-state heat conduction [39, 40]:

$$K = \frac{Q}{A}\frac{\Delta X}{\Delta T} \tag{5}$$

Here, Q represents the net heat input to the sample and is obtained as the difference between the input power with the sample and that without the sample for each measurement temperature ($Q = Q_{\mathrm{WS}} - Q_{\mathrm{WOS}}$). $A = \pi r^2$ is the cross-sectional area of the cylindrical specimen. The temperature difference is given by $\Delta T = T_2 - T_1$, measured using a datalogger, while the distance between the thermocouples is $\Delta X = X_2 - X_1$, determined from microscope photographs of the thermocouple positions.

A constant linear temperature gradient was maintained throughout the experiment using hot and cold stages. K-type thermocouples (0.5 mm diameter) were inserted into the sample to record temperature at defined positions. Heat flow was determined at each annealing temperature from repeated constant-current and voltage measurements. After completion of the thermal cycle, samples were cooled to room temperature and then sectioned transversely near the thermocouple positions. The longitudinal and transverse sections were examined to ensure the absence of porosity, cracks, or casting defects that could affect measurement accuracy. The thermal conductivity of the alloys was calculated from the measured values of A, Q, ΔT, and ΔX at each

heating step. The estimated experimental error for the longitudinal heat-flow technique is approximately 9% [23].

The temperature dependence of thermal conductivity for solid metallic materials can be expressed as:

$$K = K_0[1 - \alpha_{TTC}(T - T_0)] \quad (6)$$

where $K$is the thermal conductivity at temperature T, $K_0$is the thermal conductivity at the reference temperature T_0, and $\alpha_{TTC}$is the thermal temperature coefficient. Since $K_0 > K$, Equation (6) can be rearranged to define α_{TTC}as:

$$\alpha_{TTC} = \frac{K_0 - K}{K_0(T - T_0)} = \frac{1}{K_0}\frac{\Delta K}{\Delta T} \quad (7)$$

The slope of the thermal conductivity-temperature curve ($\Delta K/\Delta T$) is negative, and its magnitude is used to calculate α_{TTC}according to Equation (7). The temperature-dependent thermal conductivities of the Sn-Zn-Cu alloy series and pure Sn, Zn, and Cu were investigated and presented graphically.

2.4. The Enthalpy Of Fusion And The Specific Heat Change Of The Materials

Differential Scanning Calorimetry (DSC) is one of the most widely used thermoanalytical techniques for investigating the thermal behavior of materials. When a sample is heated, cooled, or held at a constant temperature, DSC measures the amount of energy absorbed or released by the material [41]. In this method, the temperature difference between the sample and a reference is monitored as a function of temperature and time. The instrument maintains both the sample and the reference at the same temperature; if a deviation occurs, the power supplied to the sample is adjusted to eliminate the difference. In this way, the heat flow associated with phase transitions can be accurately quantified.

In the present study, the melting temperatures, phase transition temperatures, and enthalpy values of four different phases in Sn-Zn-Cu solder alloys were determined using a Netzsch 449/F3 DSC system. Approximately 80 mg of material was prepared for each alloy composition. The measurements were performed under an argon atmosphere, with a heating rate of 10 K/min from room temperature up to 573 K. The resulting heat flow-temperature curves are also presented. From these curves, the onset, end, and peak temperatures as well as the transition temperature, specific heat, and enthalpy values were determined.

At constant pressure, the specific heat of a material is defined as:

$$C_p = (\frac{\partial H}{\partial T})_P \quad (8)$$

From Equation (8) [42], the enthalpy of a material taking $H = 0$ at 298 K can be obtained from:

$$H = \int_{298}^{T} C_p \, dT \quad (9)$$

At the melting temperature, the heat supplied to the system does not increase the temperature of the material [42]. Instead, this energy enables the phase transition from solid to liquid. This quantity, known as the enthalpy of fusion or latent heat of melting, is defined as:

$$\Delta H \approx \Delta C_p \, T_M \quad (10)$$

where $T_M$is the melting temperature and $\Delta C_p$is the change in specific heat across the phase transition.

3. RESULTS AND DISCUSSION

3.1. Electrical Conductivity Variation With Temperature

The electrical conductivity-temperature curves of the Sn-Zn-Cu alloys with different compositions are presented in Fig. 4. From these curves, the electrical conductivity values at the melting temperatures were determined as 4.77, 4.10, 5.20, and 5.65 ($\times 10^8$) $\Omega^{-1} \cdot m^{-1}$ for the Sn-0.28 wt.% Zn-3.6 wt.% Cu, Sn-2.56 wt.% Zn-1.38 wt.% Cu, Sn-6.77 wt.% Zn-7.18 wt.% Cu, and Sn-37.78 wt.% Zn-7.34 wt.% Cu alloys, respectively. As expected for metallic conductive systems, electrical conductivity decreases with increasing temperature due to enhanced electron-phonon scattering, as clearly shown in Fig. 4. Furthermore, the results reveal a distinct increase in electrical conductivity with increasing Cu content.

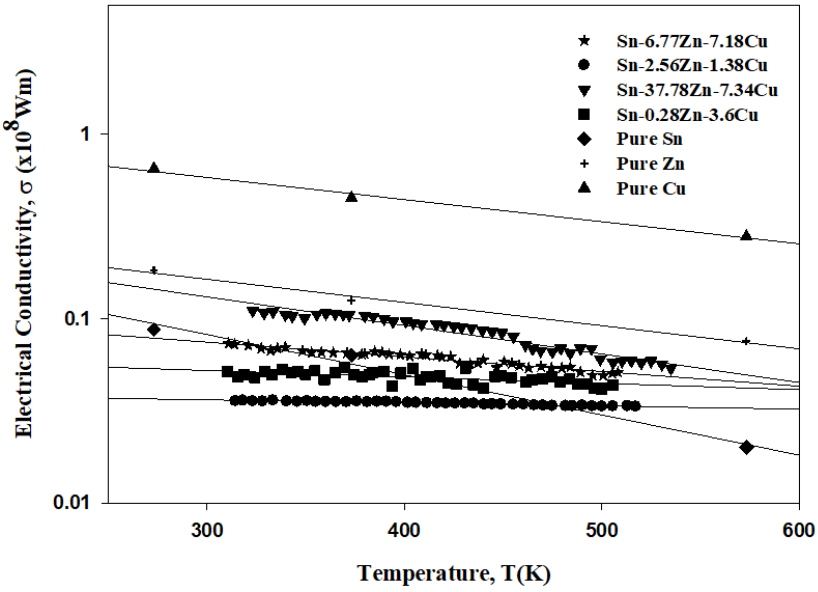

Figure 4. Electrical Conductivity-temperature graph of Sn-Zn-Cu alloy systems and Sn [43], Zn [43], Cu [43] pure metals.

Fig. 4 also compares the electrical conductivity-temperature curves of the Sn-Zn-Cu alloys with those of pure Sn [43], Zn [43], and Cu [43]. The alloy curves fall between the conductivity limits of the pure elements, with pure Cu exhibiting the highest conductivity. Consistent with this trend, the alloy containing the highest Cu concentration displayed the greatest electrical conductivity among the investigated systems. The remaining alloys showed conductivity values ranked according to their relative Cu contents.

Additionally, the temperature coefficients of electrical conductivity were obtained from the slopes of the conductivity-temperature curves. The values were calculated as 2.77, 2.81, 2.76, and 2.97 ($\times 10^{-3}$) K^{-1} for the Sn-0.28 wt.% Zn-3.6 wt.% Cu, Sn-2.56 wt.% Zn-1.38 wt.% Cu, Sn-6.77 wt.% Zn-7.18 wt.% Cu, and Sn-37.78 wt.% Zn-7.34 wt.% Cu alloys, respectively, as presented in Table 1.

Table 1. Melting temperature, electrical and thermal temperature coefficients, electrical and thermal conductivity at the melting temperature values for the Sn-Zn-Cu alloy systems

Materials (wt.%)	Melting Temperature, K	Electrical Temperature Coefficient α_{ETC} (K^{-1}) x10^{-3}	Thermal Temperature Coefficient α_{TTC} (K^{-1}) x10^{-3}	Electrical Conductivity at the Melting Temperature σ (x10^{8}/Ωm)	Thermal Conductivity at the Melting Temperature K (W/Km)
Sn-0.28wt.%Zn-3.6wt.%Cu	503	2.77	1.16	4.77	59.82
Sn-2.56wt.%Zn-1.38wt.%Cu	503	2.81	1.55	4.10	51.95
Sn-6.77wt.%Zn-7.18wt.%Cu	523	2.76	1.31	5.20	73.16
Sn-37.78wt.%Zn-7.34wt.%Cu	503	2.97	1.48	5.65	77.09

3.2. Thermal Conductivity Variation With Temperature

In Fig. 5, the thermal conductivity-temperature curves of the solid phases of the Sn-Zn-Cu alloys are presented, and the corresponding numerical values are listed in Table 1. As shown in Fig. 5, the thermal conductivity of all alloys decreases linearly with increasing temperature. The total number of phonons is proportional to temperature; therefore, above the Debye temperature (θ_D), phonon scattering becomes the dominant electron-scattering mechanism, reducing the electron mean free path. Since the specific heat $C_V$approaches the constant Dulong-Petit limit at high temperatures, the temperature dependence of thermal conductivity is primarily governed by variations in mean free path. Consequently, thermal conductivity decreases as temperature increases [44]. In alloy systems, this trend may be further influenced by compositional and microstructural differences.

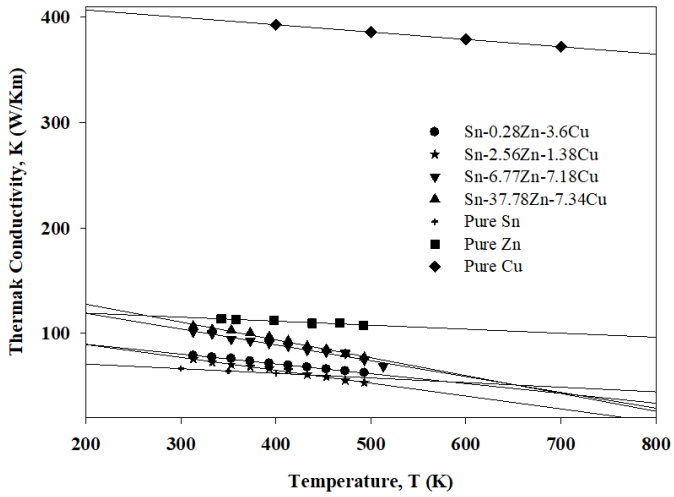

Figure 5. Thermal Conductivity-temperature graph of Sn-Zn-Cu alloy systems and Sn [39], Zn [39], Cu [39] pure metals.

As summarized in Table 1, the thermal conductivity values at the melting temperatures of the Sn-0.28 wt.% Zn-3.6 wt.% Cu, Sn-2.56 wt.% Zn-1.38 wt.% Cu, Sn-6.77 wt.% Zn-7.18 wt.% Cu, and Sn-37.78 wt.% Zn-7.34 wt.% Cu alloys were determined to be 59.82, 51.95, 73.16, and 77.09 $W \cdot m^{-1} \cdot K^{-1}$, respectively. The corresponding temperature coefficients of thermal conductivity were calculated as 1.16, 1.55, 1.31, and 1.48 ($\times 10^{-3}$) K^{-1}, as also presented in Table 1.

Fig. 5 additionally compares the thermal conductivity of the alloys with those of the pure constituent elements. The conductivity curves of the alloys lie between the values of pure Sn [39], Zn [39], and Cu [39], positioned closer to that of pure Sn. With increasing Cu content, the thermal conductivity values shift upward toward the conductivity line of pure Cu. This observation indicates that Cu is the dominant alloying element influencing both electrical and thermal transport properties in the Sn-Zn-Cu system. The increase in Cu concentration leads to enhanced thermal conductivity in the alloys. As shown in Fig. 5, the experimental results demonstrate good agreement with the known thermal conductivity values of the pure alloying elements.

3.3. The Enthalpy Of Fusion And The Specific Heat Change Of Material

Heating curves obtained from DSC measurements are highly useful for determining the reaction temperatures of materials. The endothermic peaks observed in these curves correspond to heat absorption during melting. The onset temperature (T_{onset}) represents the beginning of the endothermic reaction and marks the initial temperature at which melting starts, while the end temperature (T_{end}) indicates the completion of the melting process. During heating, T_{onset} corresponds to the solidus temperature, whereas T_{end} represents the liquidus temperature of the alloys [20]. The heating curves of the Sn-0.28 wt.% Zn-3.6 wt.% Cu, Sn-2.56 wt.% Zn-1.38 wt.% Cu, Sn-6.77 wt.% Zn-7.18 wt.% Cu, and Sn-37.78 wt.% Zn-7.34 wt.% Cu alloys are presented in Fig. 6, and the corresponding numerical values are summarized in Table 2.

Another important parameter obtained from the DSC analysis is the enthalpy of fusion of the phases. As shown in Table 2, the enthalpy values were determined to be 51.53, 57.90, 51.33, and 47.32 J/g for the Sn-0.28 wt.% Zn-3.6 wt.% Cu, Sn-2.56 wt.% Zn-1.38 wt.% Cu, Sn-6.77 wt.% Zn-7.18 wt.% Cu, and Sn-37.78 wt.% Zn-7.34 wt.% Cu alloys, respectively. The specific heat values calculated from the DSC peaks are also listed in Table 2. Among the investigated alloys, the Sn-37.78 wt.% Zn-7.34 wt.% Cu composition exhibited the lowest energy storage capacity, with a specific heat value of 0.20 J/g·°C.

Table 2. Onset temperature, peak temperature, end temperature, enthalpy, and specific heat values for the Sn-Zn-Cu alloy systems

Materials (wt. %)	Onset Temperature, T_{onset} (K)	Peak Temperature, T_{max} (K)	End Temperature, T_{end} (K)	$\Delta T=T_{end}-T_{onset}$ (K)	Enthalpy (J/g)	Specific Heat (J/gK)
Sn-0.28Zn-3.6Cu	503.10	514.40	519.50	16.40	51.53	0.21
Sn-2.56Zn-1.38Cu	511.10	518.50	523.30	12.20	57.90	0.24
Sn-6.77Zn-7.18Cu	502.10	512.70	517.90	15.80	51.33	0.21
Sn-37.78Zn-7.34Cu	500.60	515.10	521.40	20.80	47.32	0.20

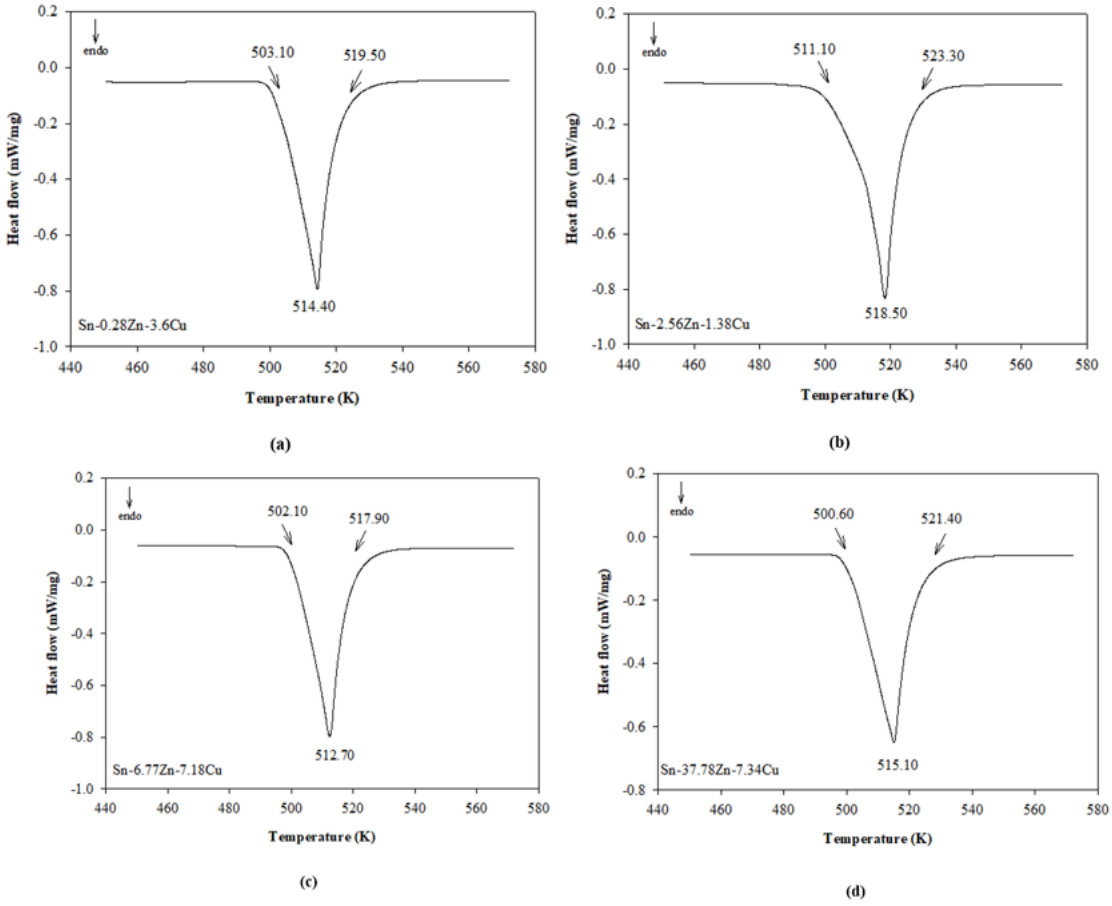

Figure 6. DSC thermogram of (a) Sn-0.28wt.%Zn-3.60wt.%Cu, (b) Sn-2.56wt.%Zn-1.38wt.%Cu, (c) Sn-6.77wt.%Zn-7.18wt.%Cu, (d) Sn-37.78wt.%Zn-7.34wt.%Cu alloy systems at heating rates of 10 ^{0}C/min.

4. CONCLUSION

In this study, four Sn-Zn-Cu alloy systems, Sn-0.28 wt.% Zn-3.6 wt.% Cu, Sn-2.56 wt.% Zn-1.38 wt.% Cu, Sn-6.77 wt.% Zn-7.18 wt.% Cu, and Sn-37.78 wt.% Zn-7.34 wt.% Cu, were examined as alternative lead-free solder candidates based on their electrical and thermal properties.

For all compositions, electrical and thermal conductivities decreased linearly with increasing temperature, ranging between 4.10-5.65 ($\times 10^8$) $\Omega^{-1} \cdot m^{-1}$ and 51.95–77.09 $W \cdot m^{-1} \cdot K^{-1}$, respectively. These transport properties exhibited strong compositional dependence: increasing Cu content led to higher conductivity values, and the conductivity trends fell between those of pure Sn, Zn, and Cu, as expected for alloy systems.

Furthermore, DSC analyses were conducted to determine melting temperatures, enthalpies of fusion, and specific heat variations. The obtained thermal data showed good agreement with previously reported values [24], confirming the reliability and reproducibility of the present measurements. Overall, the results demonstrate that Sn-Zn-Cu alloys possess favorable thermophysical behavior and exhibit strong potential as environmentally friendly lead-free solder materials suitable for various technological applications.

ACKNOWLEDGMENT

The funding of this work has provided by TÜBİTAK under Contract No: 116F010. The researchers thank to TÜBİTAK Research Foundation for their funding.

DECLARATION OF ETHICAL STANDARDS

The authors of the paper submitted declare that nothing which is necessary for achieving the paper requires ethical committee and/or legal-special permissions.

CONTRIBUTION OF THE AUTHORS

Esra Öztürk: Writing, Methodology, Data Curation, Review & Editing.
Pınar Ata Esener: Visualization, Validation, Review & Editing.
Sezen Aksöz: Visualization, Validation, Review & Editing.

CONFLICT OF INTEREST

The authors state that there is no conflict of interest to declare regarding this study.

REFERENCES

[1] Suganuma K. Advances in lead-free electronics soldering. Curr Opin Solid State Mater Sci 2001; 5: 55-64.

[2] Rashidi R, Naffakh-Moosavy H. Metallurgical, physical, mechanical and oxidation behavior of lead-free chromium dissolved Sn-Cu-Bi solders. J Mater Res Technol 2021; 13: 1805-1825.

[3] Abtew M, Selvaduray G. Lead-free solders in microelectronics. Mater Sci Eng R Rep 2000; 27: 95-141.

[4] Xing SF, Qiu X. Thermal properties, electrochemical behavior, and microstructure of Zn-5Sn-2Cu-1.5Bi-xRE high-temperature solder. J Mater Eng Perform 2015; 24: 1679-1686.

[5] Li Y, Chen C, Yi R, Ouyang Y. Special brazing and soldering: A review. J Manuf Process 2020; 60: 608-635.

[6] Xing F, Qiu XM, Li YD. Effects of Sn element on microstructure and properties of Zn-Cu-Bi-Sn high-temperature solder. Trans Nonferrous Met Soc China 2015; 25: 879-884.

[7] Lee BJ, Hwang NM, Lee HM. Prediction of interface reaction products between Cu and various solder alloys by thermodynamic calculation. Acta Mater 1997; 45: 1867-1874.

[8] McCormack M, Jin S, Kammlott GW, Chen HS. New high-strength Pb-free solder alloys based on the Sn-Ag-Zn system. Appl Phys Lett 1993; 63: 15-17.

[9] Ghosh G, Loomans M, Fine ME. An investigation of phase equilibria of the Bi-Sb-Sn system. J Electron Mater 1994; 23: 619-624.

[10] McCormack M, Jin S. New lead-free solders. J Electron Mater 1994; 23: 635-640.

[11] McCormack M, Jin S, Chen HS, Machusak DA. New lead-free Sn-Zn-In solder alloys. J Electron Mater 1994; 23: 687-690.

[12] Kattner UR, Boettinger WJ. On the Sn-Bi-Ag ternary phase diagram. J Electron Mater 1994; 23: 603-610.

[13] Loomans ME, Vaynman S, Ghosh G, Fine ME. Investigation of multi-component lead-free solders. J Electron Mater 1994; 23: 741-746.

[14] Artaki I, Jackson AM, Vianco PT. Evaluation of lead-free solder joints in electronic assemblies. J Electron Mater 1994; 23: 757-764.

[15] Kang SK, Sarkhel AK. Lead (Pb)-free solders for electronic packaging. J Electron Mater 1994; 23: 701-707.

[16] McCormack M, Jin S. Improved mechanical properties in new Pb-free solder alloys. J Electron Mater 1994; 23: 715-720.

[17] Wood EP, Nimmo KL. In search of new lead-free electronic solders. J Electron Mater 1994; 23: 709-713.

[18] Urasoğlu MG, İlbaş M. Attaining sustainable energy transition or facing costs of delayed action: A case of Turkey. Int J Energy Stud 2020; 5: 133-144.

[19] Dele-Afolabi TT, Ansari MNM, Azmah Hanim MA, Oyekanmi AA, Ojo-Kupoluyi OJ, Atiqah A. Recent advances in Sn-based lead-free solder interconnects for microelectronics packaging: Materials and technologies. J Mater Res Technol 2013; 25: 4231-4263.

[20] Choi S, Lim S, Hanifah MMM, Matteini P, Wan Yusof WY, Hwang B. An introductory overview of various typical lead-free solders for TSV technology. Inorganics 2025; 13: 86.

[21] Sobolewski M, Wojewoda-Budka J, Sobczak N, Janusz-Skuza M, Bigos A, Terlicka S, Korneva A, Szlezynger M, Adamek Z, Wierzbicka-Miernik A. Green electronics soldering by application of third generation lead-free solder alloys: Studies on their wettability and interface microstructure formed with copper. J Mater Eng Perform 2025; 34: 28134-28144.

[22] Puttlitz KJ, Stalter KA. Handbook of lead-free solder technology for microelectronic assemblies. IMB Corporation, East Fishkill, New York, 2004.

[23] Yang W, Messler RW Jr, Felton LE. Microstructure evolution of eutectic Sn-Ag solder joints. J Electron Mater 1994; 23: 765-772.

[24] Chou CY, Chen SW. Phase equilibria of the Sn-Zn-Cu ternary system. Acta Mater 2006; 54: 2393-2400.

[25] Aksöz S, Ata Esener P, Öztürk E, Maraşlı N. Effects of Bi content on thermal, microstructure and mechanical properties of Sn-Bi-In-Zn solder alloy systems. J Mater Sci Mater Electron 2022; 33: 11-26.

[26] Gündüz M, Hunt JD. The measurement of solid-liquid surface energies in the Al-Cu, Al-Si and Pb-Sn systems. Acta Metall 1985; 33: 1651-1672.

[27] Maraşlı N, Hunt JD. Solid-liquid surface energies in the AlCuAl2, AlNiAl3 and AlTi systems. Acta Metall 1996; 44: 1085-1096.

[28] Rudnev V, Loveless D, Cook R, Black M. Handbook of induction heating. Markel Dekker Inc, New York, 2003.

[29] Meydaneri F, Saatçi B, Arı M. Thermo-electrical characterization of lead-cadmium (Pb-Cd) alloys. Int J Phys Sci 2012; 7: 6210-6221.

[30] Onaran K. Material science. Science Technique Publisher, İstanbul, 2009.

[31] Ata Esener P, Bayram Ü, Öztürk E, Aksöz S, Maraşlı N. Electrical and thermal conductivity and phonon contribution to the thermal conductivity in the Bi-In system. J Therm Sci Technol 2020; 40: 367-378.

[32] Valder LB. Resistivity measurements on germanium for transistors. Proc IRE 1954; 42: 420-427.

[33] Ocak Y, Akbulut S, Keşlioğlu K, Maraşlı N. Solid-liquid interfacial energy of aminomethylpropanediol. J Phys D Appl Phys 2008; 41: 065309.

[34] Ata Esener P, Altıntas Y, Bayram Ü, Öztürk E, Maraşlı N, Aksöz S. Effect of Sn contents on thermodynamic, microstructure and mechanical properties in the Zn90-Bi10 and Bi88-Zn12 based ternary alloys. J Mater Sci Mater Electron 2019; 30: 3678-3691.

[35] Akbulut S, Ocak Y, Keşlioğlu K, Maraşlı N. Thermal conductivities of solid and liquid phases for neopentylglycol, aminomethylpropanediol and their binary alloy. J Phys Chem Solids 2009; 70: 72-78.

[36] Karadağ SB, Öztürk E, Aksöz S, Maraşlı N. Thermophysical properties of NPG solid solution in the NPG-SCN organic system. Int J Mater Res 2018; 109: 219-224.

[37] Altıntas Y, Kaygısız Y, Öztürk E, Aksöz S, Keşlioğlu K, Maraşlı N. Measurements of electrical and thermal conductivity variations with temperature and phonon component of the thermal conductivity in Sn-Cd-Sb, Sn-In-Cu, Sn-Ag-Bi and Sn-Bi-Zn alloys. Int J Therm Sci 2016; 100: 1-9.

[38] Öztürk E, Aksöz S, Keşlioğlu K, Maraşlı N. Measurement of thermal conductivity variation with temperature for Sn-20 wt.% In based lead-free ternary solders. Thermochim Acta 2013; 554: 63-70.

[39] Touloukian YS, Powell RW, Ho CY, Klemens PG. Thermal conductivity metallic elements and alloys, vol 1. New York-Washington, 1970.

[40] Kittel C. Introduction to solid state physics, 6th ed. John Wiley and Sons, 1965.

[41] Gill P, Moghadam TT, Ranjbar B. Differential scanning calorimetry techniques: Applications in biology and nanoscience. J Biomol Tech 2010; 21: 167-193.

[42] Powers JM. Department of aerospace and mechanical engineering, University of Notre Dame, USA, 2010.

[43] Mhiaoui S, Sar F, Gasser JG. Electrical and thermal conductivities and thermopower of some lead-free solders (LFS) in the liquid and solid state. J Non-Cryst Solids 2007; 353: 3628-3632.

[44] Srivastana JP. Elements of solid-state physics. Prentice Hall of India, 2006.